Characterization of Passive Fiber Resonators

Laura Wetzel
under the supervision of
Justus Schmidt and Dr. Benno Willke

Max Planck Institute for Gravitational Physics (Albert Einstein Institute), Hannover, Germany
Cornell College (Department of Physics), Mount Vernon, Iowa, USA

10 August 2015

Abstract: The utility of fiber ring resonators as optical cavities for laser frequency locking is investigated and a laser frequency control scheme exploiting the high birefringence of polarization-maintaining single-mode optical fiber to generate an error signal is tested using a 2.1 m ring cavity constructed out of SM 1064 PM fiber and a 90/10 2x2 fiber splitter. One axis of this cavity had an experimental finesse of approximately 32 and the other approximately 17. A longer ring cavity is also tested and found to have too low finesse to be practical for error signal generation.

1 Introduction

In a typical visualization of Einstein's Theory of General Relativity, spacetime is pictured as an infinite sheet in which masses move, bending the fabric of the universe like a child's weight bends a trampoline. A straight path, then, for a smaller object, becomes an orbit around a large mass; gravity's action is not so much a force as a distortion of four-dimensional spacetime.

This gravitational field can be described by the metric tensor $g_{\mu\nu}$. Naturally, when the arrangement of masses in a given system changes, this tensor must change as well, producing the new metric

$$\tilde{g}_{\mu\nu} = g_{\mu\nu} + h_{\mu\nu} \tag{1.1}$$

where $h_{\mu\nu}$ describes the perturbation to the field. In 1917, the year after he published his Theory of General Relativity, Einstein showed that the gravitational field, under the influence of this perturbation, can be described by a wave equation, and further mathematical investigation predicted that these predicted gravitational waves ought to move at the speed of light, carrying gravitational energy in a quadrupole wave and propagating through the bending of spacetime [1].

The detection and measurement of gravitational waves is the aim of much experimental and theoretical effort in current research, and justifiably so. Not only would the detection of gravitational waves serve to strengthen the Theory of General Relativity, but observation of these waves could allow probing of regions of deep space from which Earth receives limited electromagnetic radiation, either because none is radiated--as in the case of black holes--or because the region is surrounded by so much matter that most of the radiation is absorbed. Additionally, data gained from observing gravitational waves could provide insight into the origin of the universe.

1.1 Aims at detecting gravitational waves

Gravitational waves have minimal interaction with matter. This is part of what makes them useful for looking far back into the history of the universe, but it also makes them extremely difficult to detect. Efforts thus far have mainly used of two types of detectors: resonant detectors (sometimes referred to as Weber bars) and interferometers. For the sake of this paper, we are mainly concerned with interferometric detectors.

The visualization in Figure 1.1 shows the predicted effect of a gravity wave acting on a ring of particles as it propagates towards or away from the page. It is important to realize that the wave is not really "moving" the particles; rather, space itself is expanding and contracting. Nevertheless, the distance between the particles *does* change in a way that is possible to measure. An interferometric gravitational wave detector uses laser light to measure these expansions and contractions.

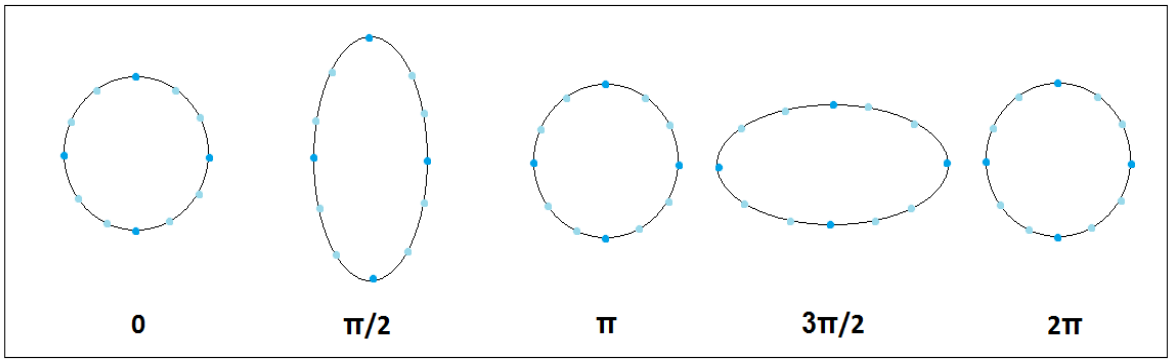

Figure 1.1 Effect of a gravitational wave on a ring of particles, through one full period.

The aphorism "Everything should be made as simple as possible, but not simpler," is commonly attributed to Einstein, so it is appropriate that the method by which the scientific community seeks to confirm his predictions conforms so well to this ideal. Interferometric detectors are based on the structure of the Michelson Interferometer, one of the most basic systems in optics. Figure 1.2 shows the typical layout of a Michelson Interferometer.

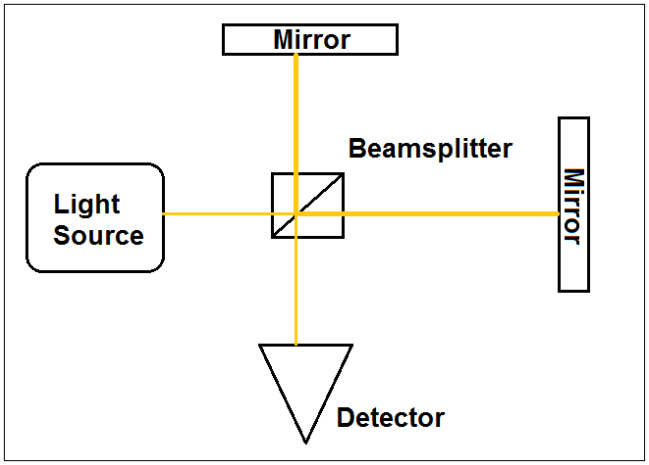

Figure 1.2 A Michelson Interferometer. Light enters the system from a light source such as a laser, and then is split by a beamsplitter into two different paths. Light from each path hits a mirror at the end of its arm, returns to the beamsplitter, and is measured at the detector, typically some sort of photodiode. Phase offset between the beams due to the differing path lengths causes interference fringes at the detector which can be used to obtain information about the frequency of the light or the difference in path length.

Interferometric detectors such as LIGO and GEO600 hope to measure the difference in arm length caused by the expansion of one arm together with the contraction of the other when a gravity wave passes through. Unfortunately, this distance change is predicted to be very tiny--on the order of 10^{-18} m, or less than 1/1000 the diameter of a proton [2]. The challenge of measuring a distance change this miniscule requires considering the "but not simpler" caveat to Einstein's aphorism.

Interferometric detectors are limited by their signal to noise ratio (SNR). Noise in the system must be reduced to a level significantly below the magnitude of the already minute

expected signal. This is no easy task, given that interferometric distance measurements are subject to noise from laser frequency and power variation, as well as to shot noise, a fundamental uncertainty in light amplitude measurements due to the particle nature of the photon. The path lengths themselves are also subject to radiation pressure noise due to high laser power, seismic noise, thermal noise, and the quantum limit, which fundamentally restricts how accurately a mirror's position can be known. For the sake of this paper, we are concerned mainly with noise due to laser frequency variation.

2 Control Theory

Fluctuations in laser frequency consist mainly of long-term drift caused by slow temperature or pressure variations in the laser's environment, and short-term fluctuations including cavity length changes due to acoustic vibrations as well as changes in the index of refraction of the lasing medium from changing acoustic pressure or discharge current [3]. Because the frequency is constantly under the influence of this noise, it is necessary to implement a control scheme to stabilize the frequency.

Figure 2.1 shows the layout of a generic control scheme. The plant produces some output which is to be stabilized. This output is measured by the sensor, and then compared to a reference to generate an error signal. The error signal is adjusted by the compensator, then fed into the actuator, which acts upon the plant to adjust the output [4].

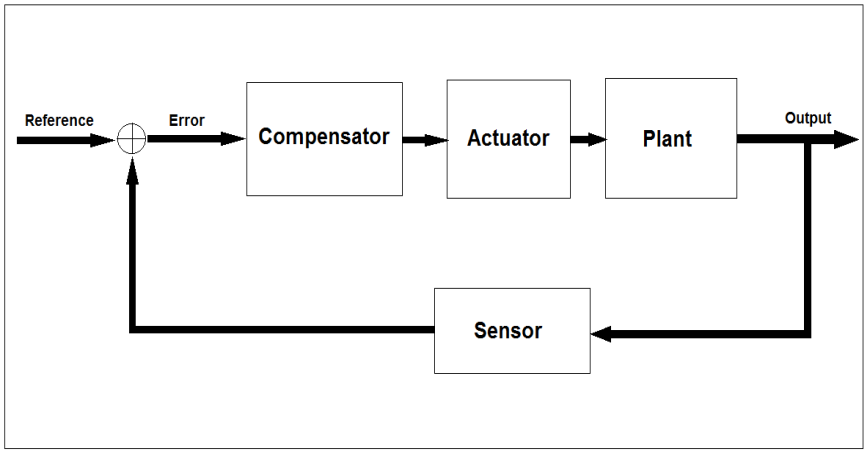

Figure 2.1 Control scheme for stabilizing the output of a generic plant.

The behavior of the control loop is governed by a series of differential equations, commonly simplified by representing inputs and impulse responses by their Laplace transforms, allowing the system to be described by a series of transfer function multiplications. Figure 2.2 shows a simplified control loop written in terms of transfer functions, with the compensator, actuator, and plant transfer functions combined and represented by G(s), and the sensor transfer function by H(s), where $s = \sigma + j\omega$, j being the imaginary number.

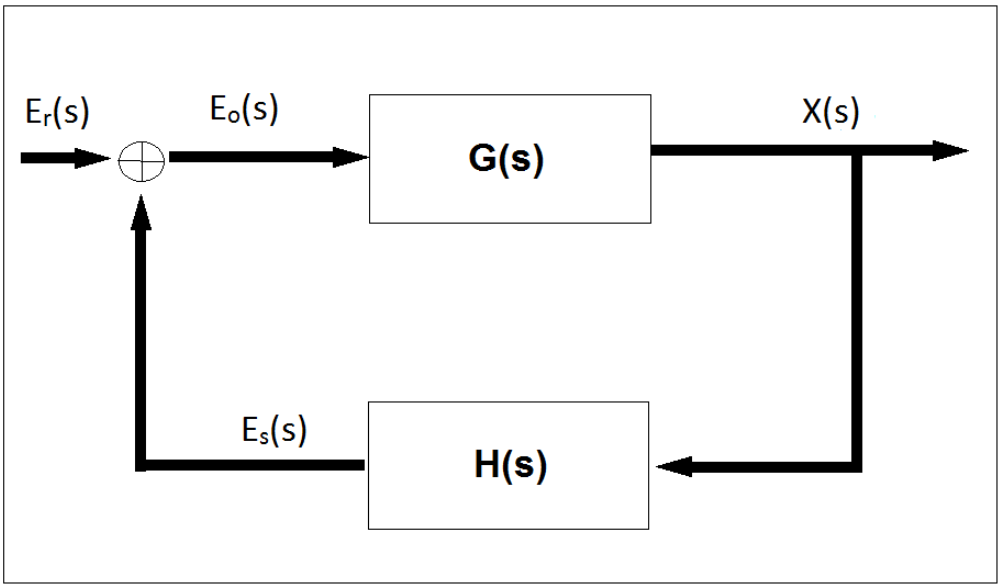

Figure 2.2 Simplified control loop.

The open-loop gain of the loop, L(s) is equal to G • H, so we can calculate

$$E_o = E_s + E_r \quad ; \quad E_s = E_o \text{ x } L \tag{2.1}$$

This becomes

$$E_o = E_r/(1 - L); \quad E_s = E_r L/(1- L) \tag{2.2}$$

In general, the higher the value of L(s), the more any noise in the circuit is suppressed. Increasing L(s), however, comes at a cost, since the slope of the plot of open-loop gain vs. frequency is related to the phase offset of the transfer function. The Nyquist Criterion for closed-loop stability requires that whenever L(s) is close to one--corresponding to a pole in (2.2)--the respective phase must be greater than -180°. Violating this criterion will lead to a system that causes the actuator to overcorrect the plant, generating oscillation in the circuit. For this reason, it is important to include reasonable margins of error to account for changes in subsystems or overlooked phase effects. These are called phase and gain margins.

2.1 Laser Stabilization and Pound-Drever-Hall

For the case of laser stabilization, the plant is the laser to be stabilized. Two main types of actuators are commonly used: temperature control, which has a wide range but acts slowly; and some sort of piezo-electric device to change the path length within the laser crystal, which has a smaller range but adjusts more quickly. In most lasers, including the Mephisto NPRO which we used for our experiments, these actuators are used together, the temperature control

countering the long-term drift, and the piezo device responding to the faster short-term fluctuations.

The sensor and the comparison to the reference signal are typically combined by the Pound-Drever-Hall method. This method relies on an optical cavity external to the laser to measure the laser frequency and generate an error signal. Often, a rigid Fabry-Perot cavity is used for this purpose. This sort of cavity consists of two flat mirrors with a constant distance between them, so that the cavity resonance frequency is a multiple of c/2L, where L, not to be confused with the open-loop gain L(s) is here equal to the distance between the mirrors, and c is the speed of light. Thus, the transmitted light is highly dependent on the frequency of the laser, creating a frequency comb (see Figure 2.3 [5]).

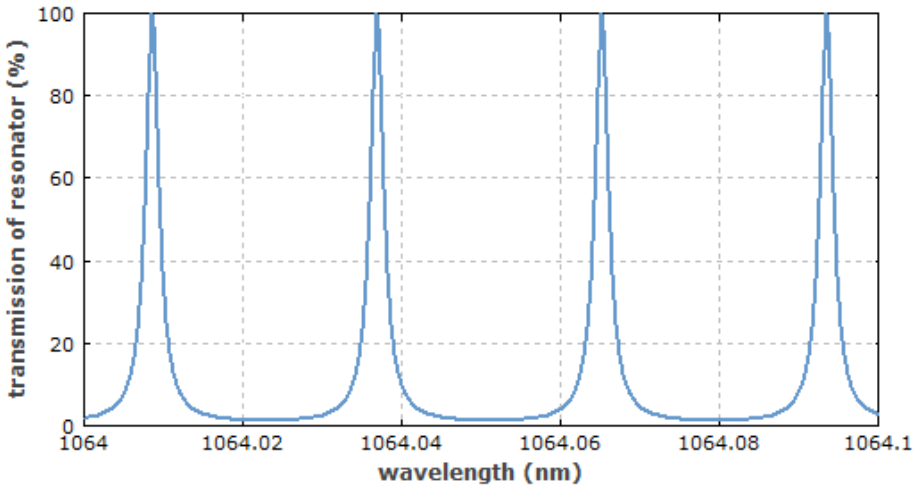

Figure 2.3 Fabry-Perot frequency comb. Transmission is plotted vs. wavelength.

One of these resonant peaks is chosen to which to lock the frequency of the laser. Note that the laser can be locked to any desired frequency within the range of the laser if the length of the cavity is chosen correctly. Also note that while Figure 2.3 shows a transmission spectrum, Pound-Drever-Hall locking is generally used instead on the reflected beam, since the reflected beam has a minimum at resonance, leading to a better SNR.

Before the beam passes through the cavity, however, it is phase modulated (e.g. by an electro-optical phase modulator), generating low amplitude sidebands on either side of the carrier frequency in the spectrum of the laser. Provided the laser frequency remains on the cavity's resonance, the effects of these sidebands will cancel each other out. If the laser frequency strays slightly to either side, however, a beating pattern will be detected at the photodiode measuring the reflected intensity. This error signal can then be fed into the compensator, allowing the control loop to perform its function of stabilizing the laser.

Since the free-running frequency stability of the Mephisto NPRO is on the order of 10^{-7}, any method to lock this laser must improve on this stability. Here, the Pound-Drever-Hall method succeeds, but it is nonetheless limited by the stability of the cavity to which the laser is

locked. For a Fabry-Perot cavity, this means the laser is still subject to noise from angular fluctuations of the mirrors forming the cavity, as well as the typical environmental influences on the optical path length within the cavity.

3 Fiber Resonators

Fiber ring resonators provide an alternative to Fabry-Perot cavities and Pound-Drever-Hall locking for use with laser stabilization. A ring resonator consists of single mode optical fiber (SMF), joined in a loop by a fiber coupler, as shown in Figure 3.1. Light from the laser to be frequency stabilized must be coupled into the input of the resonator. From there it travels through the coupler, where the cores of two optical fibers are brought very close together to allow a certain fraction of the input intensity to couple into the lower fiber. For the direct coupling resonator, this coupled light enters the fiber ring, while for the cross coupling resonator, it is the light that remains in the initial fiber that enters the ring. In either case, the laser light completes a circuit of the ring before reentering the coupler. Again, some of the intensity is transferred from one fiber to another. For the discussion of resonance, it is important to note that the coupler also introduces a 90° phase shift to the portion of the light that is coupled to the other fiber.

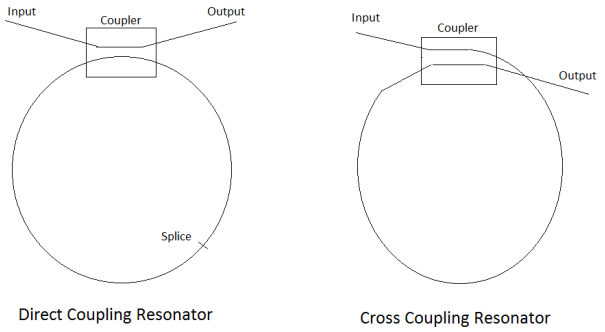

Figure 3.1 Direct coupling and cross coupling fiber ring resonators.

In order to resonate, the direct coupling ring requires a coupling coefficient κ_r, such that [6]

$$\kappa_r = 1 - (1- \gamma_0)(1- \alpha_0)e^{-2\alpha L} \quad (3.1)$$

where γ_0 is the intensity loss due to the coupler, α_0 the loss of the splice, L the length of the loop, α the loss per unit length of the fiber, and e the base of the natural logarithm [6]. In contrast, the cross coupling resonator requires [7]

$$\kappa_r = (1- \gamma_0)e^{-2\alpha L} \quad (3.2)$$

Since a system with low losses is desirable, in practice this means that the cross coupling resonator requires a very high coupling coefficient, while the direct coupling ring requires a rather low coupling coefficient. A low coupling coefficient is generally much easier to achieve than a high coupling coefficient, so the remainder of this discussion will focus on the direct coupling resonator.

Besides the correct value of the coupling coefficient, the fiber cavity also requires a particular light frequency to achieve resonance. For the direct coupling resonator, this value must satisfy

$$\beta L = 2\pi q \tag{3.3}$$

where q is an integer, and $\beta = n\omega/c$ for light of angular frequency ω in a fiber with refractive index n [6].

When both of these conditions are achieved, the light coupling from the input into the fiber ring should interfere constructively with the light already circulating the ring, leading to power build-up inside the ring. In contrast, the light flowing directly from input to output will interfere destructively with the light coupling from the ring to the output, generating a sharp negative resonance peak in the frequency spectrum of the output.

3.1 Fiber Splicing

Building a direct coupling resonator requires splicing together SMF to form a loop of fiber. For the sake of this project, a Vytran LDC-400 Cleaver was used for pre-splice cleaving of fiber, and then the fibers were spliced using a Vytran GPX-3400 Splicer. This instrument comes with a program to assist with the alignment of the fibers before the splice is completed, however, the options offered by this program are based entirely on estimating alignment of spacial characteristics. Additionally, the splice loss estimates provided by the program rely on imprecise appraisement of the core position and appear to be highly subjective. Figure 3.2 shows two images of a typical splice, together with the program's estimated loss value for each image.

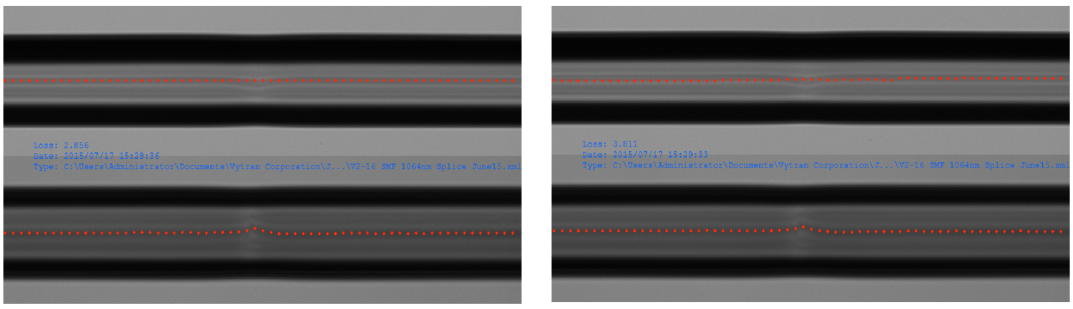

Figure 3.2 Photograph of PM 1064 SM fiber splice. The image on the right has an estimated loss of 2.856 dB, while the image on the left has an estimated loss of 3.811 dB, although both images were generated from the same splice.

To eliminate this uncertainty in loss, an active alignment process was planned for this work. The optical setup for this process appears as Figure 3.3. The beam from an NPRO laser operating at 1064 nm passes through a beam splitter and a Faraday isolator, then through a half-wave plate. It is then coupled into a single-mode polarization-maintaining fiber using a gradient index lense and an FC/APC connector. From here, the beam is moved to a separate table, where it is coupled out of the fiber by means of a collimator before passing through two additional half-wave plates and a second Faraday isolator before being coupled into the first fiber to be spliced. One end of this fiber is situated on a three-way mount to aid with alignment for coupling, while the other end is mounted in the splicer. The second fiber has one end mounted in the splicer, and the other on an out-coupling mount, so that the final beam amplitude can be measured by a photodiode sensor.

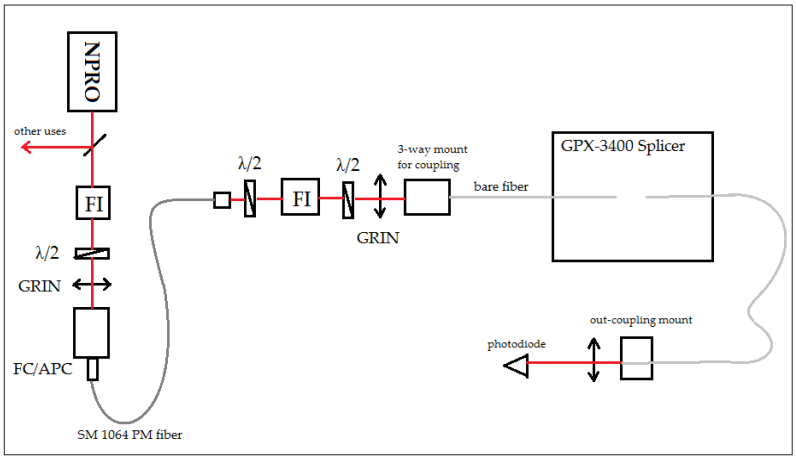

Figure 3.3 Optical setup for active splicing alignment. The photodiode power sensor used to measure the output beam was designed by Janis Wöhler and built by the author of this paper.

The rationale behind this setup is that the final beam amplitude passing through the fibers to be spliced can be measured and maximized before the splice is implemented. Additionally, the splice loss can be much more accurately calculated by comparing the amplitude of the beam passing through the fiber post-splice with the amplitude of a beam passing through a fiber of equal length that has not been spliced.

3.2 Losses and noise sources in optical fiber

Fiber cavities have many advantages over traditional interferometers such as the Fabry-Perot étalon. To list a few examples: fiber cavities are flexible and compact; the only alignment required is in- and out-coupling; light in a fiber is effectively isolated from certain types of

environmental noise--including dust particles and disturbances of air molecules--without necessitating enclosure in a vacuum chamber. However, optical fiber use is subject to unique challenges such as increased loss and noise due to Rayleigh, Raman, and Brillouin scattering.

Rayleigh scattering is a linear scattering effect that occurs due to random density fluctuations in the medium through which a beam of light is traveling. This type of scattering occurs even in the atmosphere, where it is responsible for the perceived blue color of the sky, but its effects are especially noticeable in optical fiber due to the density fluctuations that are frozen in the silica glass during fabrication [5]. Rayleigh scattering is directly proportional to laser amplitude, however, and the light is scattered mainly out the side of the fiber, so the main detrimental effect of this sort of scattering is increased loss in the fiber rather than increased noise.

In contrast, Raman and Brillouin scattering generate frequency-shifted Stokes beams that remain inside the fiber. The Raman-scattered Stokes beam propagates both forward and backward, while Brillouin scattering occurs only in the backwards direction. (This is why Brillouin scattering is sometimes referred to as "back scattering".) Raman and Brillouin scattering both occur spontaneously in optical fiber, and then are stimulated by optical or acoustic phonons, respectively, which modulate the refractive index of the fiber [10]. This process is detrimental because energy conservation stipulates that as the stimulated beam is amplified, the input beam must be attenuated. Since the spontaneous process is random, this creates an uncertainty in the output intensity of the original beam--that is to say, noise. Additionally, the scattered light is downshifted in frequency from the original wavelength, so a forward Raman-scattered beam will beat with the original beam at the output.

Fortunately, the critical power above which Raman scattering becomes a concern is much higher than in the critical power for Brillouin scattering, since Brillouin scattering involves acoustical rather than optical phonons. One reference [11] estimates 35 mW as the critical Brillouin power for a typical fiber of core area of 10^{-7} square centimeters, while the critical Raman power is estimated to be about two orders of magnitude greater. Since we are using approximately 300 mW of laser power, below the Raman threshold, Brillouin scattering is our main concern and may be responsible for some irregularities we found in our results. Due to the limited amount of time in which this project was completed, however, no thorough investigation of scattering noise was completed.

3.3 Mode-matching

It bears mentioning that one of the greatest difficulties inherent to any optical experiment is the alignment of the laser beam. In particular, the greatest difficulty we faced in implementing this experiment was the coupling of the laser beam into the optical fiber. Efficient coupling of light into optical fiber requires mode-matching of the beam to the fiber parameters. As the laser

operates in a Gaussian mode and the fundamental mode of the fiber is nearly Gaussian, it should be possible to achieve efficient coupling using a single ball lense (>90% for a low-ellipticity beam with the correct lense-to-fiber separation) [12]. Mode-matching, then, in theory, is only a question of calculating the focal length of said lense that will decrease the beam width sufficiently to optimally couple into the fiber.

Because the fibers running through our borrowed coupler terminated with fiber connectors instead of bare fiber, we were able to make use of a Schäfter and Kirchhoff Laser Beam Coupler 60SMS-1-4-A11 to simplify the task of coupling the NPRO beam into the fiber for error signal generation with our first resonator. For a fiber with a numerical aperture (NA) of 0.11, this coupler requires a nearly-collimated incident beam of diameter 1.98 mm for optimal coupling.

Measurements of the beam diameter at various points along the beam path were taken using a WINcam beam profiler. Although the beam diameter was close to the 1.98 mm specification immediately after exiting the out-coupler, it had tapered to about 1.5 mm by the point at which we considered it desirable to place the in-coupling mount. Thus, the beam came to its focus in front of the location at which the fiber's aperture was positioned, causing a low overlap integral between the laser Gaussian mode and the fiber mode, and hence, low coupling efficiency.

One way to solve this problem would have been to input our measured beam profile into a program like JamMt (Just another mode Matching tool), which would then search for a way of positioning a series of lenses in the beam path in order to adjust the profile. We found, however, that we could adjust the beam diameter by slightly changing the position of the lense in the first out-coupling mount (see Figure 4.1--this mount also used a Shäfter and Kirchhoff beam coupler, which allows for slight adjustment of the focus and tilt). By gradually optimizing this position, as well as beam-walking with the mirrors, we were finally able to achieve effective coupling of the laser to the fiber.

The frustration we faced in performing this task illustrates all the more clearly the utility of fiber-based cavities for frequency stabilization of fiber lasers. Continuous confinement of the laser beam to a fiber would save experimental scientists great amounts of time and difficulty in laser alignment.

4 Characterization of Our Resonator

Our first ring resonator was constructed using SM 1064 PM fiber with a high birefringence. We used a borrowed coupler to create this cavity, so we used fiber connectors to form the ring, rather than splicing the fiber. This coupler was a 2x2 fused PM fiber splitter with a 90/10 split ratio, giving our cavity an estimated finesse (F) of about 60, discounting

propagation losses within the fiber. The ring is approximately 2.1 m in circumference, meaning the theoretical free spectral range (FSR) is

$$FSR = c/L = 140 \text{ Mhz} \tag{4.1}$$

and the full-width half-maximum ($\Delta\nu$)

$$\Delta\nu = FSR/F = 2.3 \text{ Mhz} \tag{4.2}$$

We measured the finesse of this cavity by scanning the laser frequency over a range of (frequency range) using the fast piezo tuning capability of the NPRO laser using the set-up shown in Figure 4.1.

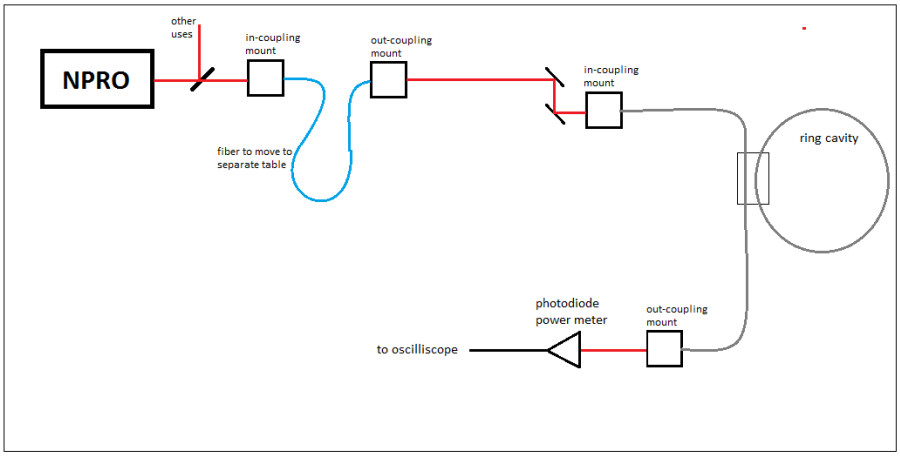

Figure 4.1 Experimental set up for cavity characterization.

Figure 4.2 displays results typical of one of these scans. As expected, the cavity's transmission is generally quite high (the photodiode we used as a power meter had a negative bias), but drops sharply to low values at the resonances. The two sets of peaks that are visible in this scan occur due to the high birefringence of the polarization-maintaining fiber. Stress members in this type of fiber create a difference in refractive index--and thus in optical length--between the fiber's "fast axis" and a "slow axis". Which path is traveled depends on the polarization of the laser beam. Thus, our fiber ring cavity can really be thought of as two separate cavities, one formed by the fiber's fast axis and the other by the slow axis.

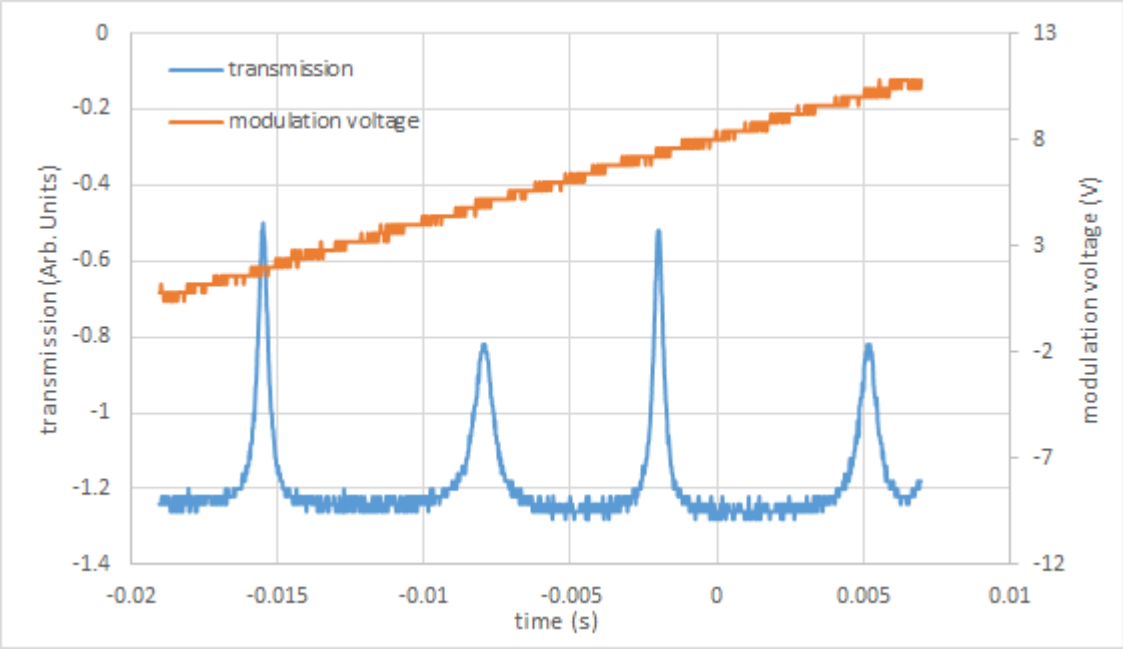

Figure 4.2 Typical frequency scan of fiber ring cavity. This scan was taken while modulating the laser frequency using a triangular wave of frequency 20 hz and peak-to-peak voltage 6 V.

Since the polarization of the laser beam entering the fiber at the time of this scan was not purely aligned to either axis, both resonances are clearly visible. These polarization-dependent cavities have approximately the same free spectral range, and the spacing between the peaks remained similar over many scans. One set of peaks, however, is much broader than the other, probably owing to higher losses experienced while travelling the slow axis of the fiber. This set of peaks and the cavity to which they correspond will henceforth be referred to as "low finesse" and the other as "high finesse". Averaging over many scans, the high finesse cavity is found to have a finesse of 32, while the low finesse cavity has a finesse of 17.

These finesses are so much lower than our theoretical value due to high losses in the connectors used to form the cavity. We predict that a cavity built using fiber splicing and a splitter with a lower coupling coefficient will exhibit a much higher finesse.

On average, the frequency passes through one free spectral range every 5.3 V. If our theoretical FSR is correct, then, we have

$$1\text{ V} \approx (1\text{ V})(140\text{ Mhz/V}) = 26\text{ Mhz} \tag{4.3}$$

according the the modulation voltage displayed in the plots. It should be noted that this voltage is only proportional to the voltage actually applied to the piezo actuator.

4.1 Time Dependence

In order to use a cavity to lock a laser beam to a certain frequency, it is evident that the error signal, and thus (for all locking schemes of which the author is aware) the resonance peaks, must occur at a stable frequency. Unfortunately, the position of the peaks with respect to the voltage ramp we used to perform our scans is not stable. The transmission signal appears to "float", bobbing slightly up and down and creeping gradually toward the peaks of the modulation voltage. Even the speed of this creep is rather unpredictable; a graph of peak position with respect to voltage over a time period of four minutes appears as Figure 4.3. A linear fit of the data (displayed for the first high finesse peak) has a slope of 2.16 V/min with coefficient of determination 0.9529.

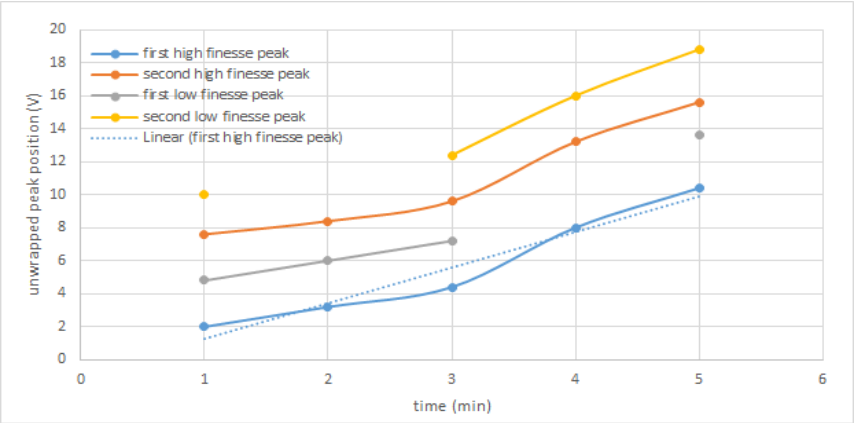

Figure 4.3 Time dependence of peak position with respect to voltage. The voltage values have been unwrapped to compensate for the finite voltage ramp.

As we were unable, during my short stay, to experimentally determine the exact laser frequency dependence on ramp voltage, it is possible that the movement of these peaks is due to hysteresis or nonlinearity in the laser frequency's response to the voltage ramp. It is also possible that the movement is due to a change in the optical length of the cavity due to heating from the gradual build-up of power within the fiber. Future experiments should be performed to address this question.

4.2 Polarization Dependence

The relative heights of the transmission peaks are, as expected, dependent upon the input polarization state. A half-wave plate was placed just in front of the transportation PM fiber and adjusted to ensure a predictable linear polarization at the output of the first out-coupling mount. An additional half-wave plate was then placed in the beam path prior to the cavity to control the orientation of this polarization. Figure 4.4 displays the dependence of peak height on the orientation of this half-wave plate.

The sinusoidal appearance of these curves makes intuitive sense if one visualizes the high and low finesse cavities as corresponding to the perpendicular and parallel components of a polarization vector moving around a circle.

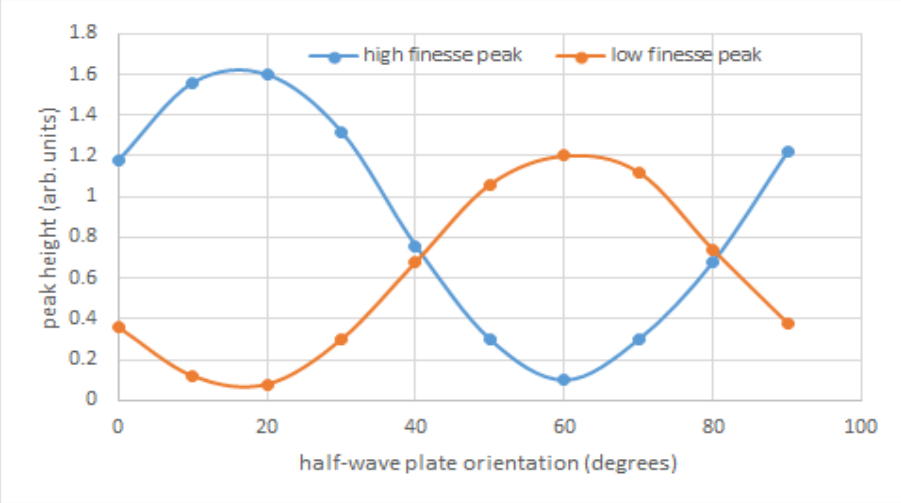

Figure 4.4 The height of resonance peaks for the high and low finesse cavities is plotted against the orientation of a half-wave plate in the beam path in front of the cavity.

To further determine the polarization dependence of our cavity, the half-wave plate was removed and replaced with a quarter-wave plate. The results of this analysis appear in Figure 4.5. As with the half-wave dependence, these curves are roughly sinusoidal, although here the high finesse peaks remain higher than the low finesse peaks. The lack of smoothness of the quarter-wave curves may be attributable to the jump in minimum voltage that occurred during the course of the measurements; thus, this voltage jump is plotted as well.

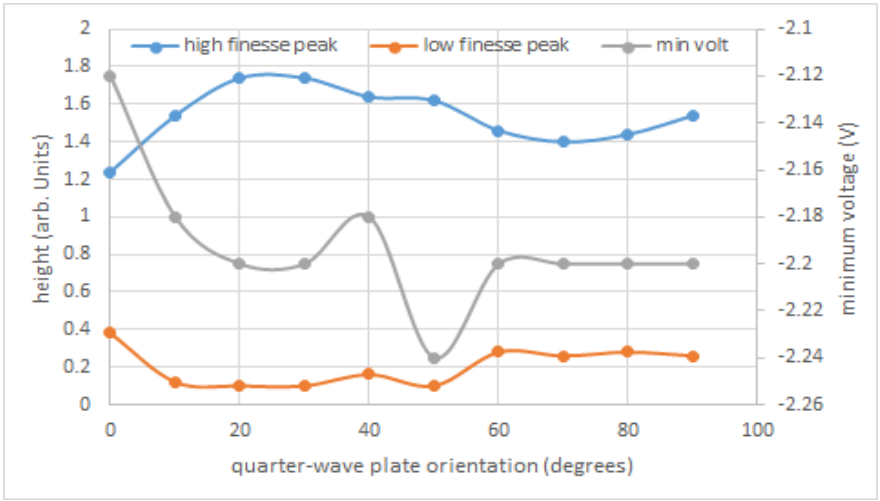

Figure 4.5 The height of resonance peaks for the high and low finesse cavities is plotted against the orientation of a quarter-wave plate in the beam path in front of the cavity. The level of maximum transmission over the course of the scan is also plotted for reference.

4.3 Length Dependence

A second cavity with ring length 7.1 m was also constructed by inserting an additional PM fiber of length 5.0 into the ring of our first cavity. This required the use of an additional fiber connector, and also increased optical path length. Thus, this cavity was expected to experience more losses than the 2.1 m cavity. A frequency scan of the 7.1 m cavity appears as Figure 4.6.

According to theory, this 7.1 m cavity would have FSR = 42 Mhz, or about 1.6 V, according to (4.3). Figure 4.6 shows about 2 V between peaks, within error margins of the theoretical value.

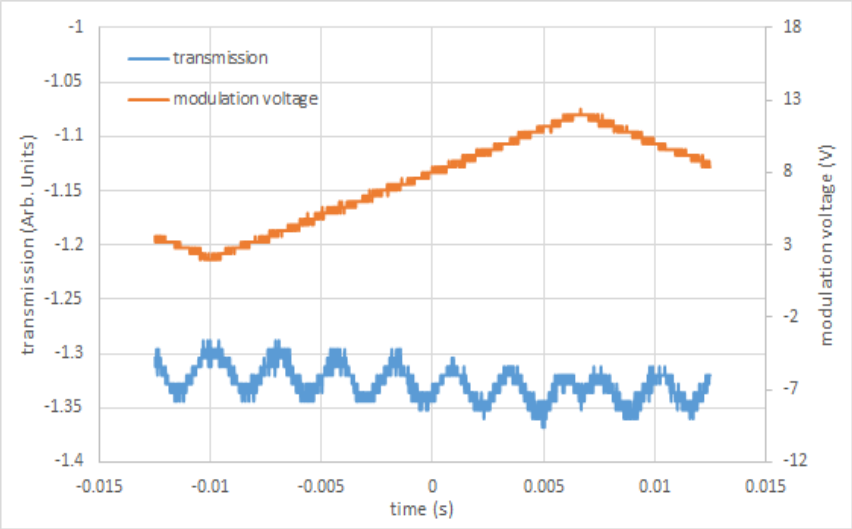

Figure 4.6 Frequency scan of 7.1 m cavity.

The calculated finesse of this cavity, however, is very low--only 1.9--indicating that this cavity is extremely lossy. A cavity with this finesse loses more than 94% of the laser power per round trip. This value seems unlikely, since the measured power through this cavity is only about 1 dB lower than the power through the 2.1 m cavity when the laser frequency is unmodulated. It is possible that one of the issues here is the resolution of the two resonance peaks. The 1.9 value for the cavity finesse was calculated from the FWHM of one of the peaks in Figure 4.6; if this broad peak is actually the combination of two resonance peaks, our calculated finesse would be about half of the actual value.

Another possible reason for this cavity's low finesse is the deviation of the splitter's coupling coefficient from the resonant value discussed in Section 3. Testing a cavity of similar length constructed using a splitter with a different coupling ratio may serve to address this question. A more thorough characterization of this longer cavity should also be completed. This

characterization should certainly investigate polarization and time dependence and perhaps also incorporate an independent way of measuring loss.

5 Generalized Hänsch-Couillard Locking

Libson et. al. [8] have suggested a technique, based on Hänch-Couillard stabilization, for generating an error signal by exploiting the birefringence of an optical cavity. This technique is particularly well-suited to fiber cavities, since its implementation does not require prior knowledge of the exact birefringent properties of the cavity. Additionally, it is much simpler than other locking techniques such as Pound-Drever-Hall, since it does not require any sort of ongoing modulation of the laser beam.

The theory behind this method requires that the polarization of the input light to the cavity must consist of an equal superposition of the eigenpolarizations of **RF**, where **R** is the amplitude reflectance Jones matrix, **F** is the cavity propagation Jones matrix, and thus **RF** represents the polarization transformation through one complete trip of the ring resonator. Because of the birefringence of the fiber, the different eigenpolarizations experience different refractive indices as they pass through the fiber, meaning that the cavity now contains two modes which will resonate at different angular frequencies. Since moving through a resonance creates a 180° phase shift in a given mode [9], there will be a significant phase difference in the modes at certain frequency values between the resonance of one mode and the resonance of the other. After the light exits the cavity, the polarization of one of these modes can be mapped (via a polarization controller) to an equal superposition of the eigenpolarizations of a given polarizing beamsplitter (PBS). This process will also shift the other mode to a polarization orthogonal to this equal superposition, but phase shifted.

An error signal, then, can be generated by comparing the power in each polarization after the light passes through the PBS. This error signal is proportional to the difference in amplitude between the two polarizations:

$$|E_1|^2 - |E_2|^2 \tag{5.1}$$

where E_1 and E_2 are the Jones vectors representing the polarization of the laser beam after passing through the second PBS in the basis of the beamsplitter eigenpolarizations. Libson et. al. have shown that, in terms of the electric field amplitude E_0 and frequency-dependent cavity eigenvalues r_a and r_b, this difference becomes

$$|E_1|^2 - |E_2|^2 = E_0^2 \mathrm{Re}\{(r_a(\omega))^* r_b(\omega) e^{i(\gamma+\varphi)}\} \tag{5.2}$$

where γ is the phase difference between the cavity eigen polarizations (generated by the birefringence), φ is a function of the pre- and post-cavity polarization controllers, Re selects the real part, and * denotes complex conjugation [8].

The optical setup we used to test Libson's method appears as Figure 5.1. In practice, it is not necessary to actually calculate the eigenpolarizations of **RF** or of the PBS; the correct polarization controller settings can be found by observing the total reflection and error signals and adjusting the polarization controllers until the signals are well balanced.

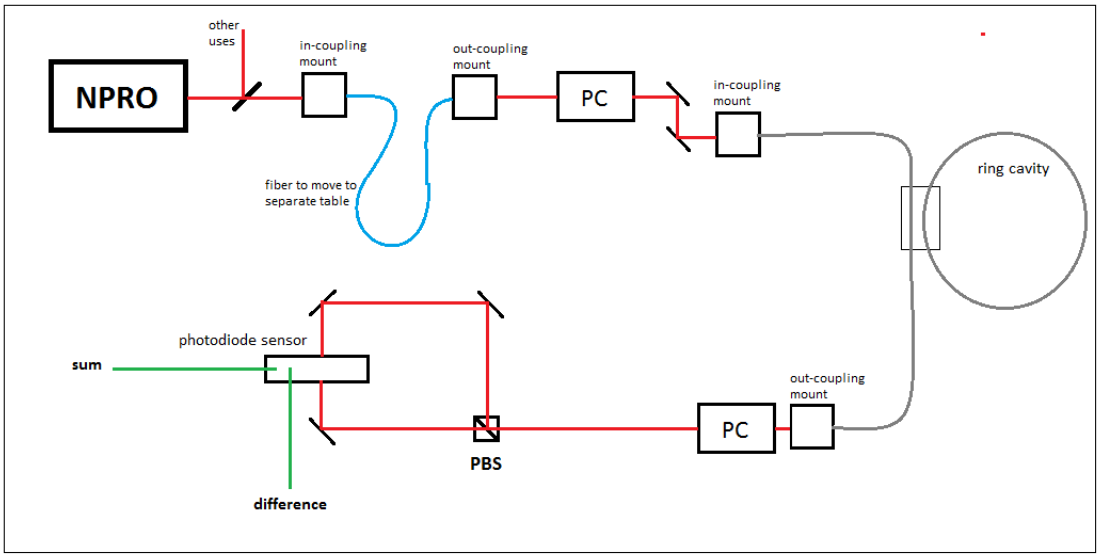

Figure 5.1 Optical setup for error signal generation. The NPRO operates at 1064 nm, and each polarization controller (PC) consists of an adjustable λ/4 plate, λ/2 plate, λ/4 plate series. Our photodiode sensor is a small homodyne detector designed by Maximillian Wimmer of the Max Planck Institute for gravitational physics.

5.2 Results

By scanning the laser frequency, we were able to generate an error signal similar to that achieved by Libson et. al, albeit less well-balanced, due to the different finesse values for the fast and slow cavities. This error signal appears in Figure 5.2. The error signal published by Libson et. al. [8] appears in Figure 5.3 for comparison.

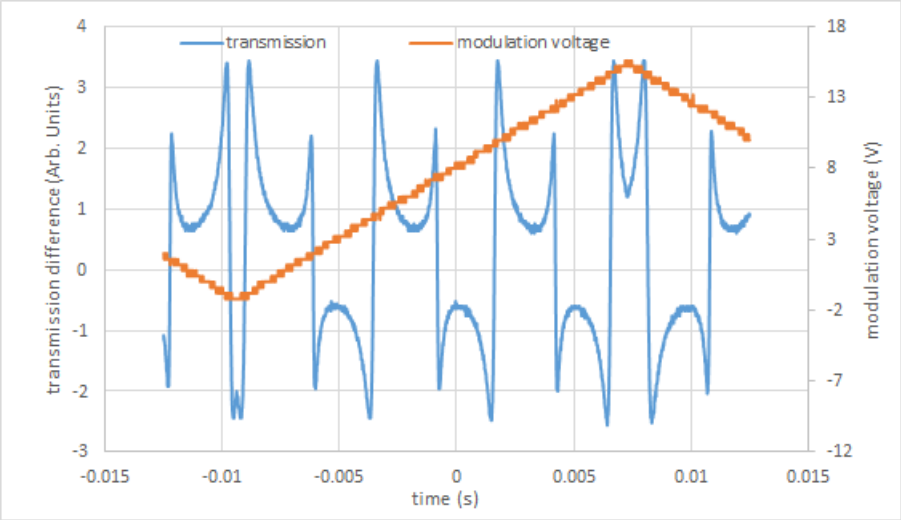

Figure 5.2 Error signal generated by scanning the laser piezo control at 30 hz with peak-to-peak amplitude 10 V.

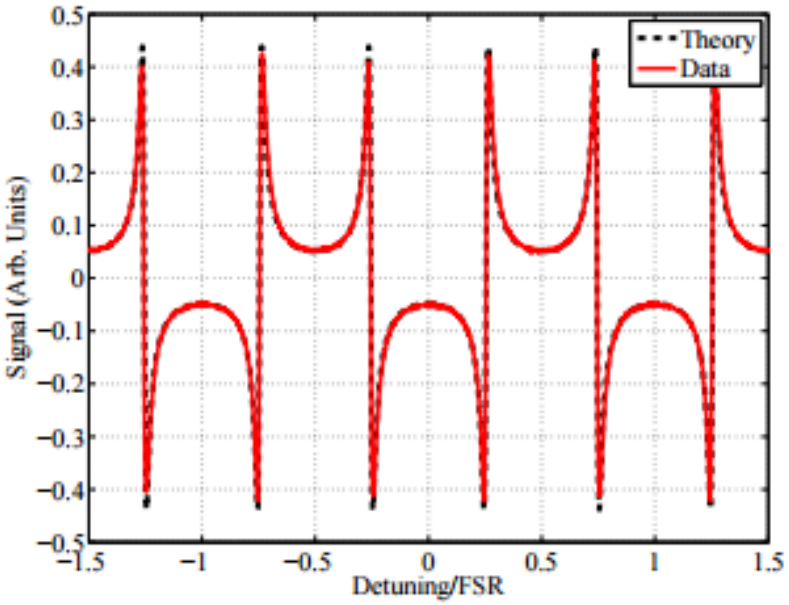

Figure 4.3 Error signal achieved by Libson et. al. [8]

Once our set-up was aligned, the generation of this error signal was the work of only a few minutes. We did not get the chance to test how well the laser could be locked to this signal, but we were impressed by the simplicity of its generation.

6 Conclusions

The ring cavity we constructed behaved according to theory, except for the strange "floating" behavior of the resonance peaks. The cause of this drift should be investigated by a

more exact characterization of the laser frequency's response to modulation of the voltage across the piezo actuator. Loss sources for the 7.1 m cavity should also be investigated, and cavities of varying lengths should be characterized when the lower coupling-coefficient splitter arrives.

As regards locking, it appears that Libson's generalized Hänsch-Couillard method is indeed relatively easy to implement using a fiber ring resonator, and even with a rather small signal passing through the cavity. Unlike the PDH method, no phase modulation is required, and Libson's method has the added advantage of allowing the signal to remain enclosed in the fiber, provided fiber-based polarization control implements are available. The elegance of using the fiber's inherent birefringence is also appreciated by the author.

Libson's locking method, and fiber ring resonators in general, hold great promise for the frequency stabilization of future fiber-based lasers, which may in time prove to improve the sensitivity of interferometric gravitational wave detectors such as LIGO and GEO600.

Acknowledgements

This project could not have been completed without the contributions of many individuals and organizations. I would first like to thank the faculty of the Cornell College Physics and Mathematics departments for teaching me so much and pushing me beyond the borders of the curriculum for every course I've taken. Special thanks to my advisor, Kara Beauchamp, for her enthusiastic support of all my endeavors.

Thanks also goes out to the University of Florida IREU program, notably to Bernard Whiting, Guido Mueller, and Kristin Nicole, for making this program possible and assigning me to a project so well suited to my interests. Additional thanks to the National Science Foundation for their generous funding.

Finally, I would like to thank all the people at the Max Planck Institute in Hannover for making my day-to-day experience so enjoyable. To Benno Willke for supervising my project, and to Justus Schmidt for answering all (most) of my questions and for being a terribly patient and terrific explainer of all the things I had yet to learn when I arrived. Also to Andreas Weidner for teaching me to solder, to Patrick Opperman for knowing everything that was going on, and to all the people who looked after me and let me into the lab on the days when Justus was absent, especially Marina Trad Nery and everyone from the Electronics Workshop.

References

[1] K.D. Kokkotas, *Gravitational Wave Physics* (2002).

[2] C. Bradaschia, and R. Desalvo, "A global network listens for ripples in spacetime", *CERN Courier* (2007).

[3] O. Svelto, *Principles of Lasers* (Springer 1998).

[4] A. Abramovici, and J. Chapsky, *Feedback Control Systems* (Kluwer Academic Publishers, 2000).

[5] R. Paschotta, *RP Photonics Encyclopedia.*

[6] F. Zhang, and J.W.Y. Lit, "Direct-coupling single-mode fiber ring resonator", *Journal of the Optical Society of America,* **5**, 1347-1355 (1988).

[7] L.F. Stokes, M. Chodorow, and H.J. Shaw, "All-single-mode fiber resonator", *Optics Letters,* **7**, 288-290 (1982).

[8] A. Libson, N. Brown, A. Buikema, C.C. López, T. Dordevic, M. Heising, and M. Evans, "Simple method for locking birefringent resonators", *Optics Express*, **23**, 3809-3817 (2015).

[9] J.E. Heebner, V. Wong, A. Schweinsberg, R.W. Boyd, and D.J. Jackson, "Optical Transmission Characteristics of Fiber Ring Resonators", *IEEE J. of Quant. Electron.* **40**, 726-730 (2004).

[10] G.P. Agrawal. *Nonlinear Fiber Optics*. Academic Press (2007).

[11] R.G. Smith. "Optical power handling capacity of low loss optical fibers as determined by stimulated Raman and Brillouin scattering", *Applied Optics.* **11**, 2489-2494 (1972).

[12] Fadhali M., Saktioto, Zainal J., Munajat Y., Ali J. and Abdul Rahman R. "Mode matching for efficient laser diode to single mode fiber coupling", *SPIE*. **6793**. 67930G-1-8 (2008).